Probabilistic calibration of material models from limited data and its influence on structural response

Conference Paper · August 2017

CITATIONS
6

READS
228

4 authors:

Aakash Bangalore Satish
Johns Hopkins University
2 PUBLICATIONS **9** CITATIONS
SEE PROFILE

Jiaxin Zhang
Oak Ridge National Laboratory
48 PUBLICATIONS **401** CITATIONS
SEE PROFILE

Pawel Woelke
Thornton Tomasetti
46 PUBLICATIONS **383** CITATIONS
SEE PROFILE

Michael Shields
Johns Hopkins University
86 PUBLICATIONS **933** CITATIONS
SEE PROFILE

Probabilistic calibration of material models from limited data and its influence on structural response

Aakash Bangalore Satish[a], Jiaxin Zhang[a], Pawel Woelke[b] and Michael D. Shields[a]
[a]Johns Hopkins University, Baltimore, USA
[b]Thornton Tomasetti Weidlinger Applied Science, New York, USA

Abstract: Most structural-scale material models are phenomenological or empirical in nature and require calibration from limited amounts of experimental data. In this paper, we present a Bayesian approach for material model calibration from limited data. The approach incorporates the uncertainties associated with both the form and the parameters of probability models for material constitutive parameters. Incorporating these effects results in an imprecise probabilistic material model that gives a more realistic assessment of the uncertainties associated with the material performance than existing calibration practices based on, for example, maximum likelihood estimation. The proposed calibration process is applied to probabilistic parameter estimation of a viscoplastic damage model for ductile metals. Specifically, the model is calibrated for aluminum alloy Al-6061 T6 at various temperatures to model structural response during fire. An experimental investigation of Al-6061 T6 at temperatures ranging from room temperature to 300°C has been conducted and the data are used for material model calibration. The material model has been implemented in Abaqus and we assess uncertainties in the tensile response of aluminum square hollow sections with an aim at placing realistic bounds on their reliability. Probabilistic structural modeling is conducted using an efficient simulation-based method for propagating the imprecise probabilities associated with material parameters.

1 Introduction

Considerable variability exists in the material properties of aluminum, especially at high temperature. This variability in the material properties is one of the factors which lead to variation in the capacity of aluminum structural members to resist imposed loads. Mechanical test data can be used to characterize the variability in the material properties. It is usually not practical to perform a large number of mechanical tests on either material test coupons or models of the structural members themselves, and hence the set of available test data is quite small in size. The small amount of data means that the uncertainty in the parameters as well as in the form of the probability model used to represent the mechanical properties is quite high. In such a scenario, it becomes necessary to devise an approach that can rationally model the uncertainty in the material parameters. One such approach as developed by the coauthors [9] is employed in this study. This method uses Bayesian inference for updating the joint distribution of the parameters of the probability models based on data, information theoretic methods for probability model selection, and importance sampling for efficient propagation of many probability models through simulations of structural response. Details of the methodology employed are presented in Sec. 3. The material behavior in these simulations is represented using a viscoplastic dam-

age model, which has several parameters needing calibration to represent the experimentally observed stress-strain behavior. Calibration of the material model is performed using a genetic algorithm and the procedure is outlined in Sec. 2. The calibrated material model is implemented in ABAQUS as a VUMAT through the WAifire module of WAimat Suite [6] and simulations of a test case of a square hollow section subjected to tension have been conducted. Since, at the time of writing, more test data was available at room temperature, the methodology was applied to this set of test data and this simple loading case as a demonstration of concept and the results are shown in Sec. 4 of the paper. Having studied this simple case allows us to investigate more complicated geometries under different conditions of loading and/or temperature.

2 Mechanical testing and material model calibration

This section provides details of the mechanical testing methodology being employed in the testing program, and of the material model and calibration procedures used.

2.1 Experiments

A series of steady state uniaxial tension tests were conducted at different temperatures on test coupons of aluminum alloy 6061-T6 to infer some of its mechanical properties. In steady state testing, the temperature and the speed of the crosshead are kept constant throughout the test. Pin-loaded tension test specimens were prepared according to specifications in ASTM E8 out of material from 5 batches sourced from two manufacturers. The length of the reduced section was 2.5 inch, width was 0.5 inch and the thickness was 0.125 inch. The test coupons were attached to the loading apparatus inside a furnace and three thermocouples were attached at the top, center, and bottom of the reduced section. Three tests were conducted from each batch of material at temperatures of 20°C, 100°C, 200°C, and 300°C. For the tests at elevated temperature, the test coupons were heated to the desired temperature and were held at that temperature for at least 20 minutes before loading. Force control was adopted during the heating phase to allow thermal expansion without stressing the material. After the specimen temperature reached equilibrium, displacement control was adopted and the crosshead was moved at a constant speed such that the nominal strain rate over a gauge length of 2 inch was 0.005 /min. Digital image correlation (DIC) was used to determine the displacement field within the specimen. To facilitate DIC, a random speckle pattern was painted using an airbrush on the surface of the test coupon and images of the deforming specimen were captured at 3 second intervals during the loading phase using a high resolution camera. The engineering stress-strain curve till failure of the test specimen was determined over a gauge length of 2 inch using the force measurements from the load cell and displacement fields calculated using DIC.

2.2 Material model

The material behavior is represented using a phenomenological damage model which is based on dilatational plasticity. The formulation given in [7] and employed in [8] is adopted and the important equations are given in this section. The plastic potential function used is dependent on the hydrostatic pressure and is given by

$$f = \sqrt{J_2 + n\xi I_1^2} \tag{1}$$

where, J_2 is the second invariant of the deviatoric stress tensor, n is the strain hardening exponent, ξ is the damage variable which is a scalar parameter controlling the softening behavior of the material and I_1 is the first invariant of the stress tensor. The evolution of the damage variable is given by the equation

$$d\xi = K d\varepsilon_{kk}^{p+} \tag{2}$$

where, K is a calibration function and $d\varepsilon_{kk}^{p+}$ is the expansive volumetric plastic strain. The yield condition is given by

$$F = \frac{f}{k} - 1 = 0 \tag{3}$$

where, k is the isotropic hardening function given by

$$k = k_0 + k_\infty \int s_{ij} d\varepsilon_{ij}^{dev,p} \tag{4}$$

where $k_0 = \sigma_y/\sqrt{3}$, σ_y is the tensile yield stress, and $d\varepsilon^{dev,p}$ is the incremental deviatoric plastic strain. The associated flow rule to obtain the plastic strain increments is

$$d\varepsilon^p = d\lambda \frac{\partial F}{\partial \boldsymbol{\sigma}} \tag{5}$$

and the elastic constitutive law is given by

$$d\boldsymbol{\sigma} = \boldsymbol{E}(d\boldsymbol{\varepsilon} - d\boldsymbol{\varepsilon}^p) \tag{6}$$

where additive decomposition of the total strain tensor is made as $d\boldsymbol{\varepsilon} = d\boldsymbol{\varepsilon}^e + d\boldsymbol{\varepsilon}^p$. The plastic multiplier is obtained by satisfying the consistency requirement and is given by

$$d\lambda = \frac{\left(\frac{\partial F}{\partial \boldsymbol{\sigma}}\right)^T \boldsymbol{E} d\boldsymbol{\varepsilon}}{\left(\frac{\partial F}{\partial \boldsymbol{\sigma}}\right)^T \boldsymbol{E} \frac{\partial F}{\partial \boldsymbol{\sigma}} - \left(\frac{\partial F}{\partial k}\right)^T k_\infty \boldsymbol{s}^T \frac{\partial F}{\partial \boldsymbol{s}} - \left(\frac{\partial F}{\partial \xi}\right)^T K \frac{\partial F}{\partial I_1}} \tag{7}$$

The elasto-plastic stiffness is given by

$$\boldsymbol{D} = \boldsymbol{E}\left[\boldsymbol{I} - \frac{\left(\frac{\partial F}{\partial \boldsymbol{\sigma}}\right)^T \boldsymbol{E} \frac{\partial F}{\partial \boldsymbol{\sigma}}}{\left(\frac{\partial F}{\partial \boldsymbol{\sigma}}\right)^T \boldsymbol{E} \frac{\partial F}{\partial \boldsymbol{\sigma}} - \left(\frac{\partial F}{\partial k}\right)^T k_\infty \boldsymbol{s}^T \frac{\partial F}{\partial \boldsymbol{s}} - \left(\frac{\partial F}{\partial \xi}\right)^T K \frac{\partial F}{\partial I_1}}\right] \tag{8}$$

2.3 Calibration

For the case of uniaxial tension, the stress tensor is given by

$$[\boldsymbol{\sigma}] = \begin{pmatrix} \sigma(t) & 0 & 0 \\ 0 & 0 & 0 \\ 0 & 0 & 0 \end{pmatrix} \tag{9}$$

where, $\sigma(t)$ is the engineering stress given by $\sigma(t) = F(t)/A_0$ where $F(t)$ is the force measured by the load cell and A_0 is the initial cross sectional area of the test specimen. For isotropic material and small strains the total strain tensor is given by

$$[\boldsymbol{\varepsilon}] = \begin{pmatrix} \varepsilon(t) & 0 & 0 \\ 0 & -\nu(t)\varepsilon(t) & 0 \\ 0 & 0 & -\nu(t)\varepsilon(t) \end{pmatrix} \tag{10}$$

where $\nu(t) = \frac{\varepsilon_{lat}(t)}{\varepsilon_{long}(t)}$ is the lateral contraction coefficient, where the longitudinal and lateral strains are calculated using DIC. The elastic strain tensor is given by

$$[\boldsymbol{\varepsilon}^e] = \begin{pmatrix} \frac{\sigma(t)}{E} & 0 & 0 \\ 0 & -\nu\frac{\sigma(t)}{E} & 0 \\ 0 & 0 & -\nu\frac{\sigma(t)}{E} \end{pmatrix} \tag{11}$$

where ν is the Poisson's ratio and E is the Young's modulus. The deviatoric stress tensor is calculated using the stress tensor as $s_{ij} = \sigma_{ij} - \frac{1}{3}\delta_{ij}\sigma_{kk}$ and the plastic strain tensor can be calculated using the additive decomposition of the total strain tensor. Substituting for the deviatoric stresses, and plastic strains and simplifying, the yield condition, Eq. (3), becomes

$$\frac{\sigma\sqrt{\frac{1}{3}+n\xi}}{k_0+k_\infty\int\frac{2}{3}(1+\nu)\sigma d\varepsilon^p} - 1 = 0 \tag{12}$$

The calibration function is given by

$$K = k_1 \exp\left(k_2\frac{\varepsilon^p_{eq}}{N}\right) \tag{13}$$

where, k_1 and k_2 are calibration constants, ε^p_{eq} is the equivalent plastic strain given by $\varepsilon^p_{eq} = \sqrt{\frac{2}{2}\varepsilon_{ij}\varepsilon_{ij}}$ and N is the strain at the onset of necking. K is used in Eq. (2) to calculate the increment in the damage variable. The equations (2) and (12) are used in the model calibration process to calculate the stresses predicted by the model to input plastic strains, conditioned on the value of the calibration constants. The optimal values of the calibration constants are identified by solving an unconstrained optimization problem using a genetic algorithm (GA). The objective is to minimize the norm of the difference between the experimental stress-strain curve and the stress-strain curve obtained from the material model given by

$$\min_{k_1,k_2}\sqrt{\sum_{\varepsilon^p}\left(\sigma_{mod}(\varepsilon^p,\sigma_y,N,k_1,k_2)-\sigma_{exp}(\varepsilon^p)\right)^2} \tag{14}$$

This calibration process is conducted to match each experimentally obtained stress-strain curve. The values of σ_y, N, and ε^p are obtained directly from the experimental data.
The only variables in the optimization process are k_1 and k_2. The lower and upper bounds of the values of these variables are set as 0 and 16 respectively and the individual string length was such that a precision of better than 0.01 was achieved in the values of these variables. The GA as implemented uses an elitist strategy with binary tournament selection, uniform crossover with probability 0.5, and a high mutation probability of 0.1 to balance the high selection pressure caused by using an elitist strategy. The population size used was 250 and the number of generations was 50. The entire process was repeated 30 times for each experiment and it was seen that convergence was obtained in all the 30 cases to almost the same values of k_1 and k_2. The values of k_1 and k_2 which provided the best fitness was used and these values of k_1 and k_2, along with N define the value of the damage variable at failure.
The values of the material parameters σ_y, N, k_1, k_2 and ξ_{max} were slightly different from each test, conducted at the same temperature, indicative of the variability in these parameters. These values were used as the input to the multimodel selection process and Bayesian importance sampling, as outlined in Sec. 4.

3 Review of Bayesian importance sampling from limited data

This section provides a brief review of Bayesian importance sampling used for material model calibration from limited data. The approach incorporates the uncertainties associated with both the form and the parameters of probability models for material constitutive parameters. Incorporating these effects results in an imprecise probabilistic material model that gives a more realistic assessment of the uncertainties associated with the material performance. One can find more details in [9].

3.1 Bayesian inference

Bayes' rule provides a means of updating the knowledge of the parameters $\boldsymbol{\theta}$ for probability model M using collected data $\boldsymbol{d}$. A posterior distribution $p^*(\boldsymbol{\theta}|\boldsymbol{d},M)$ reflecting our updated knowledge is defined based on the data $\boldsymbol{d}$ and prior information, denoted $p(\boldsymbol{\theta};M)$, that reflects our current belief or knowledge,

$$p^*(\boldsymbol{\theta}|\boldsymbol{d},M) = \frac{p(\boldsymbol{d}|\boldsymbol{\theta},M)p(\boldsymbol{\theta};M)}{p(\boldsymbol{d};M)} \propto \mathscr{L}(\boldsymbol{\theta}|\boldsymbol{d},M)p(\boldsymbol{\theta};M) \tag{15}$$

where $\mathscr{L}(\boldsymbol{\theta}|\boldsymbol{d},M) = p(\boldsymbol{d}|\boldsymbol{\theta},M)$ is the likelihood function and the normalizing factor $p(\boldsymbol{d};M)$, referred to as the evidence, is computed by marginalizing $\mathscr{L}(\cdot)$ over the parameters $\boldsymbol{\theta}$

$$p(\boldsymbol{d};M) = \int \mathscr{L}(\boldsymbol{\theta}|\boldsymbol{d},M)p(\boldsymbol{\theta};M)d\boldsymbol{\theta} \tag{16}$$

Since the integral is usually analytically intractable, the Markov Chain Monte Carlo (MCMC) method is employed to draw samples from $p^*(\boldsymbol{\theta}|\boldsymbol{d},M)$. Here we use the affine invariant ensemble sampler for MCMC proposed by Goodman and Weare [3].

3.2 Multimodel selection and model uncertainty

Traditionally, statistical inference is applied to determine a single "best" model, that is the sole model for making inference from data. However, any uncertainty associated with model selection is ignored as a single best model has been found. In the limited dataset, rather than very large datasets, it is intractable to identify a unique best model. Therefore, a process referred to as multimodel inference [2] becomes necessary to quantify the model uncertainty and compare the validity of multiple candidate models.

An appropriate model selection criteria is to minimize the information loss based on the information-theoretic framework. Akaike [1] presented that the expected relative Kullback-Leibler (K-L) information could be approximated by the maximized log-likelihood function with a bias correction. Based on this relation, Akaike established the Akaike Information Criterion (AIC). For small datasets, a criterial extension of the AIC has been developed [5, 4] as

$$\mathrm{AIC}_c = -2\log(\mathscr{L}(\hat{\boldsymbol{\theta}}|\boldsymbol{d},M)) + 2K + \frac{2K(K+1)}{n-K-1} \tag{17}$$

which should be used when $\frac{n}{K} <\sim 40$ and is generally more accurate than the classical AIC regardless of dataset size.
It is useful to develop a relative scale for AIC_c values such that:

$$\Delta_A^{(i)} = \mathrm{AIC}_c^{(i)} - \mathrm{AIC}_c^{\min} \tag{18}$$

where the best model has $\Delta_A^{(i)} = 0$ and all other models with positive $\Delta_A^{(i)}$ are interpreted as the information lost relative to the best model. Normalizing the likelihoods using a simple transformation $\exp(-\frac{\Delta_A^{(i)}}{2})$, we can estimate the model probabilities as

$$\mathfrak{p}_i = p(M_i|d) = \frac{\exp(-\frac{1}{2}\Delta_A^{(i)})}{\sum_{i=1}^{N}\exp(-\frac{1}{2}\Delta_A^{(i)})} \tag{19}$$

In this study, AIC_c is utilized for multimodel selection given small dataset. Probability models are ranked with respect to $\Delta_A^{(i)}$ and model probabilities assigned according to Eq. (19).

3.3 Importance sampling and the selection of an optimal sampling density

We now focus on the issue of efficient uncertainty propagation given the parametric and model-form uncertainties created by small datasets. To achieve the simultaneous propagation of many possible target models, we utilize the principles of importance sampling and derive an optimal sampling density for a set of plausible probability models.

3.3.1 Importance sampling

Given the performance function $g(\boldsymbol{X})$, the problem of uncertainty propagation is generally to evaluate the expected value $E[g(\boldsymbol{X})]$ where $\boldsymbol{X} \in \Omega$ is a random vector having probability model $M_{\boldsymbol{X}}$ with density function $p(\boldsymbol{x})$. The classical Monte Carlo estimator is given by:

$$E_p[g(\boldsymbol{X})] = \int_{\Omega} g(\boldsymbol{x}) p(\boldsymbol{x}) d\boldsymbol{x} \approx \frac{1}{N} \sum_{i=1}^{N} g(\boldsymbol{x}_i) \tag{20}$$

where $E_p[\cdot]$ is the expectation under $p(\boldsymbol{x})$, $\boldsymbol{x}_i$ are independent random samples drawn from $p(\boldsymbol{x})$, and N is the number of samples. It is sometimes beneficial to draw samples from an alternate density $q(\boldsymbol{x})$ such that the Monte Carlo estimator becomes

$$E_q\left[g(\boldsymbol{X})\frac{p(\boldsymbol{X})}{q(\boldsymbol{X})}\right] = \int_{\Omega} g(\boldsymbol{x})\frac{p(\boldsymbol{x})}{q(\boldsymbol{x})} q(\boldsymbol{x}) d\boldsymbol{x} \approx \frac{1}{N}\sum_{i=1}^{N} g(\boldsymbol{x}_i)\frac{p(\boldsymbol{x}_i)}{q(\boldsymbol{x}_i)} \tag{21}$$

where $E_q[\cdot]$ is the expectation with respect to $q(\boldsymbol{x})$. The ratios $w(\boldsymbol{x}_i) = p(\boldsymbol{x}_i)/q(\boldsymbol{x}_i)$ is defined as the importance weights, that will play an essential role in the proposal approach. This process is referred to as importance sampling and a critical challenge is to identify the "best" $q(\boldsymbol{x})$.

3.3.2 Optimal sampling density for multiple distributions

Much research has been conducted toward identifying an efficient proposal sampling density $q(\boldsymbol{x})$ if the target density $p(\boldsymbol{x})$ is exactly known. However, the target density $p(\boldsymbol{x})$ is not known exactly in the case of imprecise probabilities.

Instead, multiple probability models, M_i, are plausible, each with density functions identified through multimodel inference (Eq. (19)) and uncertain parameters $\boldsymbol{\theta} \in \Theta \subseteq \mathbb{R}^d$, quantified through Bayesian inference. This work aims to identify a *single* sampling density $q^*(\boldsymbol{x})$ that is representative of all plausible $p_i(\boldsymbol{x}|\boldsymbol{\theta})$ and can be used with importance sampling to simultaneously propagate the full set of candidate probability models. We are interested in ensuring that our sampling density is as close as possible to the target densities. This is achieved by minimizing the mean square differences (MSD) defining the difference between two distributions P and Q over a space Ω as:

$$\mathscr{M}(P \parallel Q) = \frac{1}{2}\int_{\Omega} \left(p(\boldsymbol{x}) - q(\boldsymbol{x})\right)^2 d\boldsymbol{x} \tag{22}$$

Consider that we have a finite set $\mathbb{M} = \{M_i\}, i = 1,2,...,N_d$ of candidate target probability models having densities $p_i(\boldsymbol{x}|\boldsymbol{\theta})$. Thus the total expected mean squared differences can be defined as:

$$E\left[\mathscr{M}(\mathbb{M} \parallel Q)\right] = \sum_{i=1}^{N_d} E\left[\mathscr{M}(M_i \parallel Q)\right] = E_{\theta}\left[\int_{\Omega}\sum_{i=1}^{N_d}\frac{1}{2}(p_i(\boldsymbol{x}|\boldsymbol{\theta}) - q(\boldsymbol{x}))^2 d\boldsymbol{x}\right] \tag{23}$$

An overall optimization problem aims to minimize the expected mean square differences given

the isoperimetric constraint as

$$\begin{aligned} \underset{q}{\text{minimize}} \quad & \hat{T}(q) = E_\theta \left[\int_\Omega \hat{F}(\boldsymbol{x}, \boldsymbol{\theta}, q(\boldsymbol{x})) d\boldsymbol{x} \right] \\ \text{subject to} \quad & \hat{I}(q) = \int_\Omega q(\boldsymbol{x}) d\boldsymbol{x} - 1 = 0 \end{aligned} \tag{24}$$

where the action functional $\hat{F}$ is:

$$\hat{F}(\boldsymbol{x}, \boldsymbol{\theta}, q(\boldsymbol{x})) = \frac{1}{2} \sum_{i=1}^{N_d} \left(p_i(\boldsymbol{x}|\boldsymbol{\theta}) - q(\boldsymbol{x}) \right)^2 \tag{25}$$

We define the Lagrangian associated with the objective functional $\hat{T}(q)$ and the constraint $\hat{I}(q)$, then vanish all variations δq, $\delta \lambda$

$$\begin{aligned} \delta \hat{L}(q, \lambda) &= \delta \hat{T}(q) + \delta(\lambda \hat{I}(q)) \\ &= E_\theta \left[\int_\Omega \left(\frac{\partial \hat{F}}{\partial q}(\boldsymbol{x}, \boldsymbol{\theta}, q(\boldsymbol{x})) + \lambda \right) d\boldsymbol{x} \right] \delta q + \left(\int_\Omega q(\boldsymbol{x}) d\boldsymbol{x} - 1 \right) \delta \lambda \end{aligned} \tag{26}$$

which leads to $\int_\Omega q(\boldsymbol{x}) d\boldsymbol{x} = 1$ and

$$E_\theta \left[\frac{\partial F}{\partial q}(\boldsymbol{x}, \boldsymbol{\theta}, q(\boldsymbol{x})) + \lambda \right] = E_\theta \left[-\sum_{i=1}^{N_d} \left(p_i(\boldsymbol{x}|\boldsymbol{\theta}) - q(\boldsymbol{x}) \right) + \lambda \right] = 0 \tag{27}$$

Solving for $q(\boldsymbol{x})$ gives the minimizer that is the optimal sampling density:

$$\hat{q}^*(\boldsymbol{x}) = \frac{1}{N_d} \left(\sum_{i=1}^{N_d} E_\theta \left[p_i(\boldsymbol{x}|\boldsymbol{\theta}) \right] - \lambda \right) \tag{28}$$

Which leads to $\lambda = 0$ such that $\int_\Omega q^*(\boldsymbol{x}) d\boldsymbol{x} = 1$. The final optimal sampling density is therefore,

$$\hat{q}_T^*(\boldsymbol{x}) = \frac{1}{N_d} \sum_{i=1}^{N_d} E_\theta \left[p_i(\boldsymbol{x}|\boldsymbol{\theta}) \right] \tag{29}$$

The solution in Eq. (29) is a mixture distribution combining the candidate target densities and their parameter ranges. It is straightforward to show that this solution generalizes as:

$$\hat{q}_T^*(\boldsymbol{x}) = \frac{1}{N_d} \sum_{i=1}^{N_d} E_\theta \left[\mathfrak{p}_i \cdot p_i(\boldsymbol{x}|\boldsymbol{\theta}) \right] \tag{30}$$

where $\mathfrak{p}_i$ is the AIC_c model probability (see Eq. (19)) for model M_i satisfying $\sum_{i=1}^{N_d} \mathfrak{p}_i = 1$.

4 Application

For demonstration purposes, the proposed method is shown here for uncertainty in yield strength only. Extension to uncertainty in the full damage model follows in a straightforward way. The minimum design value for yield stress of aluminum alloy A1-6061 is $\sigma_0 = 35000$ psi so that we define a random variable $\hat{\sigma}_0$ as the deviation from this minimum value as $\hat{\sigma}_0 = \sigma_0 - 35000$. From the tension test results, we collect 13 yield stress data, as shown in Fig. 1. These serve as

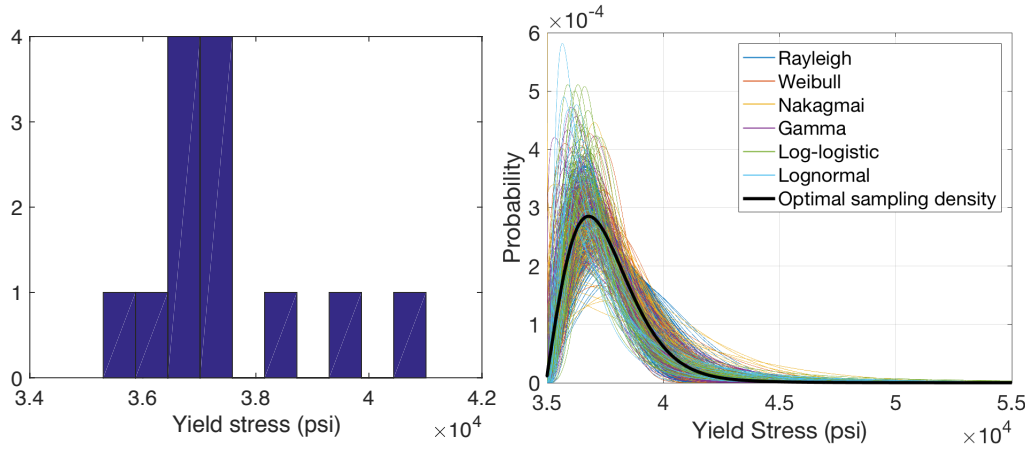

(a) (b)

Figure 1: (a)13 yield stress values that serve as the initial dataset for uncertainty quantification and propagation in material model calibration, and (b) Candidate pdfs and the optimal sampling density from 13 yield stress values

the initial data from which uncertainty will be quantified and propagated. Clearly, a probability model form cannot be precisely identified from these limited data.

The minimum yield stress provides a lower-bound that we assume is strictly enforced. This enables us to consider only probability models with support on the positive real line $(0,\infty)$. The AIC_c model selection criteria is employed to rank the candidate distributions as shown in Table 1. The top six probability models with $\Delta_A^{(i)} < 5$ have significant probability of being the "best" model. Meanwhile, the last three models are removed since they have much larger AIC_c values and very low probabilities. Thus, the top six probability models are selected to represent the limited dataset.

Table 1: Ranked candidate probability models based on AIC_c *given 13 yield stress values*

Rank	Distribution	AIC_c	$\Delta_A^{(i)}$	$\mathfrak{p}_i$
1	Rayleigh	225.76	0.000	0.471
2	Weibull	228.33	2.57	0.130
3	Nakagami	228.41	2.66	0.125
4	Gamma	228.49	2.73	0.120
5	Log-logistic	228.89	3.13	0.098
6	Lognormal	230.71	4.95	0.040
7	Inverse Gaussian	232.45	6.69	0.017
8	Levy	243.83	18.08	5.59e-05
9	F	286.99	61.23	2.38e-14

Using MCMC, Bayesian inference from a uniform prior is used to estimate the joint posterior parameter distribution for the six models. The six probability models with their joint parameter distributions are then discretized to create a finite set of models using the Monte Carlo method. The probability model is randomly selected based on the AIC_c probabilities $\mathfrak{p}_i$ in Table 1.

Fig. 1(b) shows 1000 candidate densities for the yield stress drawn from the model set. The optimal sampling density $q_T^*(\boldsymbol{x})$ is determined analytically as a mixture of these candidate

density using Eq. (29) and is presented as the thick black line in Fig. 1(b). Then the cloud of distributions in Fig. 1(a) are propagated using importance sampling reweighting 1000 samples generated from $\hat{q}_T^*(\boldsymbol{x})$. Figure. 2(a) shows the cumulative distribution functions for the maximum tensile force in an aluminum tube section, highlighting the range of probabilistic response resulting from both parametric and model-form uncertainties created by limited dataset for the yield stress. The variations between colors stand for the model-form uncertainty while the variations with a single color represents the parametric uncertainties for a given model-form. Figure. 2(b) and (c) shows CDFs of the mean and standard deviation of the maximum force respectively as well as the overall CDF considering all probability models as shown by the thick black line in the figure.

The probability of failure issue is also investigated to study the effects of model-form and parametric uncertainty. We consider three cases where "failure" is assumed to occur when the maximum force is less than 13000 lbf, 14000 lbf and 14400 lbf respectively. Therefore, the empirical CDFs for probability of failure are shown in Fig. 3. These figures also present the overall CDF as well as the conditional CDFs given specific probability model with different colors.

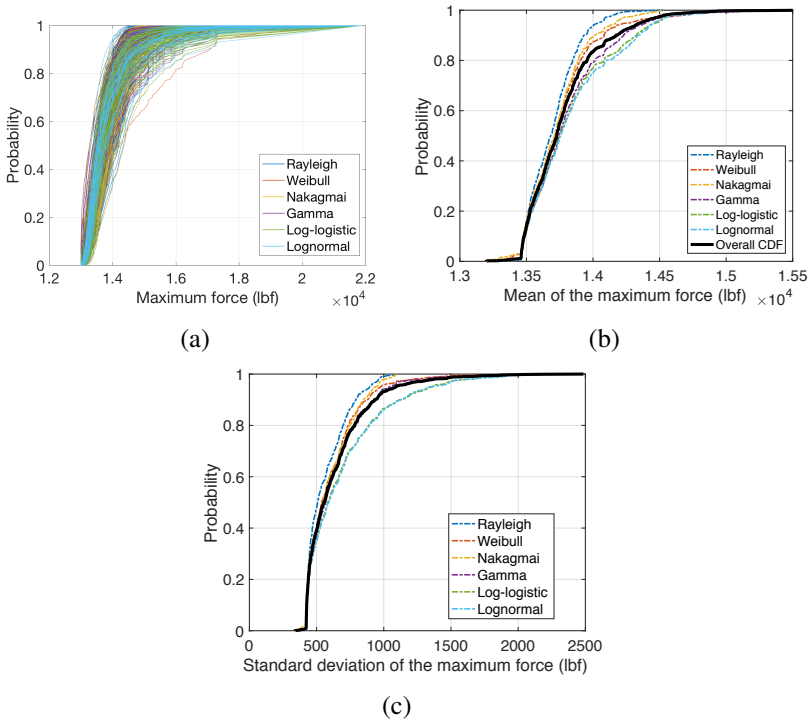

Figure 2: (a) Collection of candidate empirical CDFs for maximum force, (b) empirical CDFs for the mean of the maximum force, and (c) empirical CDFs for the standard deviation of the maximum force

A similar investigation has been conducted to study the total energy which is another important probabilistic response. The empirical CDFs as well as the mean and standard deviation are shown in Fig. 4.

Acknowledgement

The work presented herein has been supported by the Office of Naval Research under Award Number N00014-16-1-2754 with Dr. Paul Hess as program officer and by the National Science Foundation under grant number CMMI-1400387 with Y. Grace Hsuan as Program Officer.

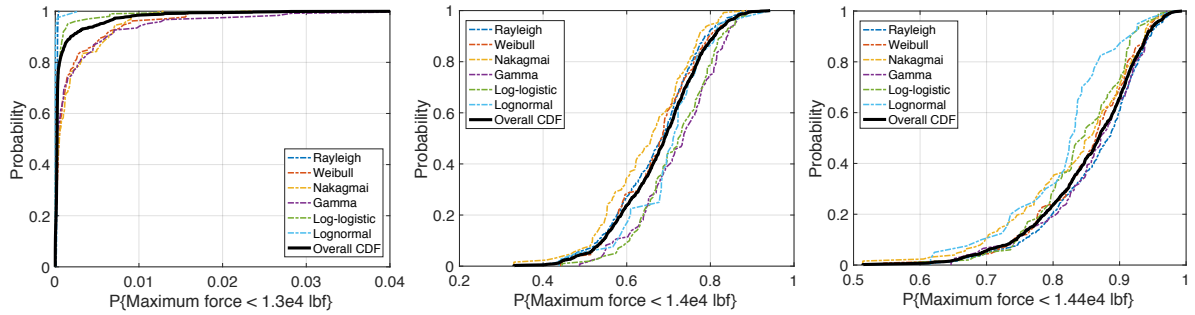

(a) (b) (c)

Figure 3: Empirical CDFs for the probability of failure occurs when (a) maximum force $<$ 13000 *lbf, (b) maximum force* $<$ 14000 *lbf, and (c) maximum force* $<$ 14400 *lbf.*

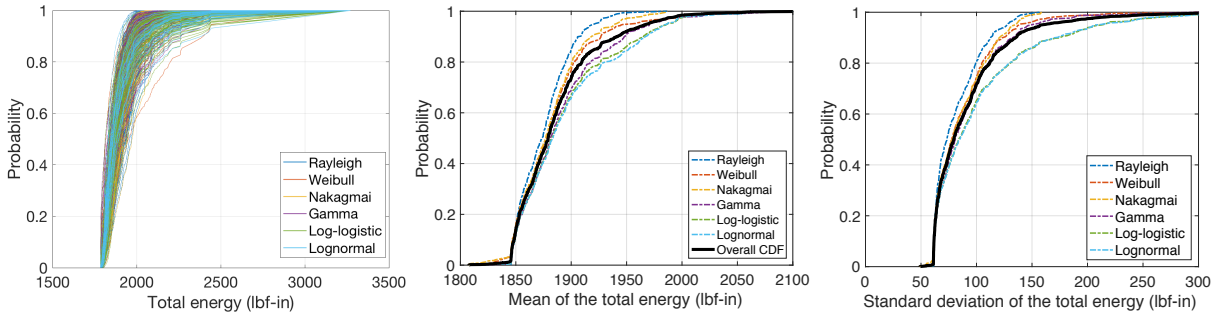

(a) (b) (c)

Figure 4: (a) Collection of candidate empirical CDFs for total energy, (b) empirical CDFs for the mean of the total energy, and (c) empirical CDFs for the standard deviation of the total energy

References

[1] H. Akaike. "A new look at the statistical model identification". In: *IEEE transactions on automatic control* 19.6 (1974), pp. 716–723.

[2] K. P. Burnham and D. R. Anderson. "Multimodel inference understanding AIC and BIC in model selection". In: *Sociological methods & research* 33.2 (2004), pp. 261–304.

[3] J. Goodman and J. Weare. "Ensemble samplers with affine invariance". In: *Communications in applied mathematics and computational science* 5.1 (2010), pp. 65–80.

[4] C. M. Hurvich and C.-L. Tsai. "Model selection for extended quasi-likelihood models in small samples". In: *Biometrics* (1995), pp. 1077–1084.

[5] C. M. Hurvich and C.-L. Tsai. "Regression and time series model selection in small samples". In: *Biometrika* 76.2 (1989), pp. 297–307.

[6] Thornton Tomasetti Inc. *WAimat Suite*. URL: `http://www.waimat.com`.

[7] P. B. Woelke and N. N. Abboud. "Modeling fracture in large scale shell structures". In: *Journal of the Mechanics and Physics of Solids* 60.12 (2012), pp. 2044–2063.

[8] P. B. Woelke et al. "Simulations of ductile fracture in an idealized ship grounding scenario using phenomenological damage and cohesive zone models". In: *Computational Materials Science* 80 (2013), pp. 79–95.

[9] J. Zhang and M. D. Shields. "On the quantification and efficient propagation of imprecise probabilities resulting from small datasets". In: *Mechanical Systems and Signal Processing* 98 (2018), pp. 465-483.